Agricultural and Forest Meteorology 389 (2026) 111451

Contents lists available at ScienceDirect

Agricultural and Forest Meteorology

journal homepage: www.elsevier.com/locate/agrformet

Weak sensitivity of annual N_2O emission to precipitation in a paddy-dominated agricultural landscape

Jie Shi [a], Mi Zhang [a,*], Wei Xiao [a,b], Yanhong Xie [c], Yang He [d], Hengxin Bao [e,f], Fuyu Yang [a], Shenbao Zhang [a], Xuhui Lee [g,*]

[a] Yale-NUIST Center on Atmospheric Environment, Collaborative Innovation Center on Forecast and Evaluation of Meteorological Disasters, Nanjing University of Information Science & Technology, Nanjing, Jiangsu, PR China
[b] State Key laboratory of Climate System Prediction and Risk Management, Nanjing University of Information Science & Technology, Nanjing, Jiangsu, PR China
[c] Guangxi Zhuang Autonomous Region Ecological and Environmental Monitoring Center, Nanning, Guangxi, PR China
[d] Liaoning Agricultural Meteorology and Satellite Remote Sensing Center, Shenyang, Liaoning, PR China
[e] Hebei Xiong'an New Area Meteorological Bureau, Xiongan, Hebei, PR China
[f] CMA Xiong'an Atmospheric Boundary Layer Key Laboratory, Xiongan, Hebei, PR China
[g] School of the Environment, Yale University, New Haven, CT, USA

ARTICLE INFO

Keywords:
Annual N_2O emission
Paddy-dominated agricultural landscape
Precipitation
Hot moment

ABSTRACT

Agriculture is the largest anthropogenic source of atmospheric N_2O. Dryland crops are known to emit disproportionately large amounts of N_2O in short hot moments and to display high interannual variability in the emission rate. In comparison, the temporal dynamics of paddy rice N_2O emission are less well understood. In this study, the N_2O flux was measured near-continuously using an eddy covariance system on a 70-m tall tower in a paddy-dominated agricultural landscape of the Yangtze River Delta, China from 2019 to 2024. The results showed that hot moment occurrence time fraction was higher in the month of fertilization (June; 33%) than the average across the full year (14%), but hot-moment fluxes were not as well-defined as those reported for dryland crops. The six-year mean N_2O flux was 8.5 kg N_2O—N ha^{-1} yr^{-1}. The annual flux was weakly correlated with annual precipitation (linear correlation= +0.63, p = 0.18). The coefficient of variation (CV) of the annual N_2O emission (5.9%) was much smaller than the CV of precipitation (25.1%), indicating weak sensitivity of the N_2O flux to precipitation. The overall emission factor, calculated as the ratio of N in the annual N_2O flux to the flux footprint-weighted N fertilizer input, was 4.3% ± 0.2%, which is much higher than the IPCC direct (dryland crops: 1%; paddy fields: 0.4%) and indirect emission factor (1.1%) for paddy rice. Future work should investigate if this high emission factor also holds for paddy rice in other climate zones and under different water management regimes.

1. Introduction

Nitrous oxide (N_2O) has a global warming potential approximately 300 times that of carbon dioxide (CO_2) over a 100-year timescale (Griffis et al., 2017). N_2O concentration in the atmosphere is increasing at an annual rate of about 2% per decade (Tian et al., 2020). Being the largest anthropogenic source of N_2O, the agricultural sector contributes 3.6 Tg N yr^{-1} or 56% of the global anthropogenic N_2O emissions (Tian et al., 2024). This emission estimate has a large uncertainty range from 2.7 to 4.8 Tg N yr^{-1}. This uncertainty stems from three major challenges that confront local emission measurements and calculations. First, in an agricultural ecosystem, N_2O is emitted directly from cropland fertilizer use and livestock manure. N_2O is also indirectly emitted from waters surrounding croplands, where approximately 30% of nitrogen fertilizers enter via runoff and leaching (IPCC, 2006). However, indirect N_2O fluxes remain difficult to measure and model due to the episodic nature of the emission and high spatial heterogeneity across agricultural landscapes (Griffis et al., 2013).

Second, a cropland ecosystem often shows short-term high N_2O emission fluxes. These episodic high fluxes are referred to as hot moments (McClain et al., 2003; Bernhardt et al., 2017; Wagner-Riddle et al., 2020). They typically account for only 1% to 10% of the observation period but can contribute over 50% of the total annual N_2O emission. Hot moments are evident in high-frequency time series of the

* Corresponding authors.
E-mail addresses: zhangm.80@nuist.edu.cn (M. Zhang), xuhui.lee@yale.edu (X. Lee).

https://doi.org/10.1016/j.agrformet.2026.111451
Received 31 March 2026; Received in revised form 10 July 2026; Accepted 23 August 2026
Available online 1 September 2026

N_2O flux observed with eddy-covariance (EC) and flux chambers (Stuchiner et al., 2025; Li et al., 2015; Scanlon and Kiely, 2003; Molodovskaya et al., 2012; Barczyk et al., 2024). Because their episodic nature – some last <24 h – they may evade detection if measurement frequency is too low. Hot moments are also difficult to model. For example, the DNDC model successfully simulated the total N_2O emission in an agricultural landscape in Canada, but it was less accurate in predicting the timing and the magnitude of hot moments (Desjardins et al., 2010). To complicate the matter further, N_2O emission is highly variable in space in an agricultural landscape which typically consists of multiple crop types with heterogenous fertilizer management practices. A hot moment captured in one crop field may not be representative of its neighboring fields. It remains unclear whether the significant contribution of N_2O hot moments, observed at the plot (~10 m) and the field scale (~100 m), also holds true at the landscape scale (~10 km).

Third, observational studies published so far have shown that N_2O emission can be highly variable interannually. The coefficient of variation (CV) often exceeds 20% (Anthony and Silver, 2021; Barczyk et al., 2024; Li et al., 2015; Tallec et al., 2022; Wagner-Riddle et al., 2007) and sometimes reaches 106% (Merbold et al., 2021). Evidence suggests that this emission variability is linked to precipitation variability (e.g., Haszpra et al., 2018; Desjardins et al., 2010). By increasing soil moisture, precipitation creates anaerobic conditions, which enhances denitrification and leads to increased N_2O production and emission (Chen et al., 2017; Wang et al., 2024). Precipitation may also enhance indirect N_2O emission by increasing nitrogen loss from runoff and leaching (Wang et al., 2023). Notably, most multi-year observations are restricted to dryland ecosystems dominated by maize, wheat and rapeseed. N_2O emission from persistently wet soils is negligible because strongly reducing conditions promote the complete reduction of N_2O to N_2 (Kroon et al., 2010; van Beek et al., 2011). However, even though paddy soil is flooded, with fertilizer N input, and water-level management, rice paddies can sustain N_2O production and emission through dynamic redox conditions (Cai et al., 1997). It is unclear if N_2O emission in paddy-dominated agricultural landscapes varies significantly at the interannual timescale and if the annual N_2O emission exhibits similar precipitation sensitivity to that of dryland crops.

The main N_2O emission pathway is nitrogen fertilizer application in cropland. China is the largest consumer and producer of nitrogen fertilizer in the world. In 2022, China used 49 million tons of nitrogen fertilizer, accounting for about 37% of the global total in the same year. The Yangtze River Delta (YRD) stands out as one of the most intensively cultivated regions in the country. This study focuses on a paddy-dominated agricultural landscape in the YRD. In this landscape, paddy fields constitute 72.7% of the land area and rely heavily on nitrogen fertilizer to sustain high crop yield. We conducted long-term, high-frequency, and continuous N_2O flux measurement with an EC system on a 70-m tall tower. We aim to: (1) investigate the contribution of hot moments to the N_2O emission and factors influencing hot moments, (2) examine monthly, seasonal and annual emission patterns, and (3) quantify the interannual variations of N_2O emission in relation to precipitation.

2. Methods

2.1. Site description

The EC tower was located in Quanjiao County, Anhui Province in the YRD (31.9667°N, 118.2607°E). The region is under of the influence of subtropical monsoon climate. The annual mean temperature and the precipitation are 16.1 °C and 1091 mm, respectively. The landscape within the 5-km radius of the tower is composed of paddy cultivation (72.7%), dryland (wheat and maize, 1.1%), forests (10.2%), fishponds (4.2%), other water bodies (5.0%), sealed area (5.1%) and other land cover types (wetland, grassland, shrubland and bare land, 1.7%) according to the 10-meter spatial resolution land cover map provided by Gong et al. (2019). Paddy cultivation consists of rice-fallow rotation, rice-wheat rotation, rice-shrimp farming, and vegetable farming. The paddy was transplanted in May and harvested in October, with conventional water management involving early-season flooding, mid-season drainage, and moderate irrigation without waterlogging in the late season. Nitrogen fertilization consisted of compound fertilizers and urea. For paddy, compound fertilizers were applied as a basal fertilizer prior to transplanting, followed by urea topdressing between June and early July. For wheat, application occurred twice in a crop season, once in November and the other time in February of the following year. For fishpond, fingerlings were stocked in the in early February and harvested in January of the next year. From May to November, formulated feed was applied at a frequency of two to three times per day. Large quantities of chicken manure were incorporated as supplementary feed in the initial and mid-to-late phases.

The annual N input in the paddy cropland in the EC footprint was estimated to be 160 kg N ha^{-1} yr^{-1} in 2019, based on the data provided by local farmers (Xie et al., 2022). This estimate was a weighted mean N input to rice-fallow rotation (110 kg N ha^{-1}; areal percent: 40%), rice-wheat rotation (160 kg N ha^{-1}; areal percent: 30%), rice-shrimp farming (240 kg N ha^{-1}; areal percent: 25%), and vegetable farming (160 kg N ha^{-1}; areal percent: 5%). The annual N inputs for subsequent years were scaled from the 2019 value using the year-specific relative changes in N input at the county level using county level data provided by the provincial government (https://tjj.chuzhou.gov.cn/). The annual N input were estimated as 156, 153, 129, 139, and 135 kg N ha^{-1} yr^{-1} from 2020 to 2024, respectively. This scaling assumes that the county-level statistics accurately reflected year-to-year fluctuations in N fertilizer use by the local farmers. The aquaculture ponds in the landscape primarily practiced a fish-mussel polyculture. The annual N input of the aquaculture ponds from 2019 to 2024 was 1430, 1752, 1203, 1819, 1651 and 1322 kg N ha^{-1}, respectively.

2.2. EC flux and microclimate measurements

A closed-path EC system was installed on a free-standing tall tower at the height of 70 m above the ground (Fig. S1). The EC system consisted of a closed-path CO_2/N_2O gas analyzer (Model TGA200A, Campbell Scientific Inc., Logan, Utah, USA) and a three-dimensional ultrasonic anemometer (Model CSAT3B, Campbell Scientific Inc.). The EC system was oriented at azimuth angle of 35° into the prevailing wind. Installed in July 2018, it commenced normal observation in October 2018. The EC system signals were sampled at 10 Hz and stored by a datalogger (model CR6, Campbell Scientific Inc.). The high frequency data were used to compute half-hourly fluxes. Details of the sampling setup of the closed-path EC system, including a schematic diagram, cell pressure, pump type, tube type and length, flowrate, and calibration procedure, are provided by Xie et al. (2022).

Microclimatic variables were sampled at 1 Hz and were averaged to half-hourly means by two dataloggers (model CR3000/CR1000, Campbell Scientific Inc.). Air temperature and humidity were measured with temperature/humidity sensors (model HMP155, Vaisala Inc., Helsinki, Finland) at the heights of 10, 50 and 70 m above the ground. Wind speed and direction were measured with anemometers and wind vanes (model 05,103, R M Young Inc., Traverse City, Michigan, USA) at the heights of 10 m and 50 m above the ground. Solar radiation was measured with a four-component radiometer (model CNR4, Kipp & Zonen B.V., Delft, the Netherlands) at the height of 10 m above the ground. Air pressure was measured with a pressure senor (model CS106, Campbell Scientific Inc.) at the height of 70 m above the ground. Soil temperature (T_{soil}) at soil depth of 10 cm was measured with a temperature sensor (T109, Campbell Scientific Inc.).

Precipitation data was obtained from a standard weather station which belongs to the China Meteorological Data Network. It was located in Chuzhou City, approximately 30 km northeast of the study site.

2.3. EC data processing

Half-hourly fluxes were calculated with the EddyPro software (Version 6.2.1, LI-COR Inc.) Before the flux calculation, statistical tests were performed on the 10 Hz raw data to screen and remove spikes (Vickers and Mahrt, 1997). A double coordinate rotation was used to correct sensor tilt (Aubinet et al., 2012). Spectral corrections were implemented to compensate for high-frequency flux losses caused by sensor separation and line averaging (Moncrieff et al., 1997). The time lag introduced by the spatial separation between the gas analyzer and the three-dimensional sonic anemometer and the closed-path sampling tube was accounted for (Xie et al., 2022).

The eddy fluxes were corrected for storage in the air column below the measurement height using the concentration time series measured by the analyzer. Following the quality flag system of Mauder and Foken (2004), only observations with flags 0 and 1 were retained, while those with flag 2 were excluded. The N_2O flux was constrained to a range of −10 to 30 nmol m^{-2} s^{-1} and the CO_2 flux to −50 to 50 μmol m^{-2} s^{-1}. Nighttime N_2O and CO_2 flux data was excluded if the friction velocity fell below 0.1 m s^{-1} (Aubinet et al., 2012).

Our analysis focused on the fluxes at the daily, monthly and annual timescales. A daily mean N_2O flux was calculated when >50% of the half-hourly data within a day were valid. The proportion of valid daily mean flux ranges from 51.1% (2020) to 75.3% (2019). A monthly mean N_2O flux was calculated when over 50% of the days had valid daily flux in the month. There were 54 months, or 75%, with valid monthly N_2O flux during 2019–2024. Missing months were gap-filled using an air temperature and precipitation predictive model proposed by (Xie et al., 2022).

Regarding the CO_2 flux data, daytime gap fraction varied from 34.6% (2019) to 54.2% (2020), and the nighttime gap fraction (after friction velocity screening) varied from 32.9% (2019) to 60.1% (2022). An exponential relationship between valid half-hourly nighttime CO_2 flux and 10-cm soil temperature was used to calculated ecosystem respiration (RE). Gross primary production was calculated as GPP = RE − NEE, where NEE is net ecosystem exchange (i. e., the EC flux corrected for storage).

2.4. Calculation of the N_2O emission factor

The half-hourly flux footprint was calculated using the flux footprint prediction model of Kljun et al. (2015). To calculate the N_2O emission factor, we aggregated fertilizer usage data to the eddy flux footprint. The flux contribution density was combined with a 10-meter spatial resolution land cover map (Gong et al., 2019) to determine the weighting factor of each land cover type. Paddy cropland and fishpond were the only land use types in the EC footprint subject to fertilizer application. The cropland footprint weight was 67.5% (range from 66.8% to 68.2%) and the fishpond weight was 5.7% (range from 5.2% to 5.9%). The emission factor was determined as the ratio of the total annual N_2O flux to the footprint-weighted N input. This calculation was performed for each year.

2.5. Detection of hot moment

The two most common methods for detection of hot moment involve standard deviation and 75%-to-25% inter-quantile range (IQR; Stuchiner et al., 2025). A detection threshold is chosen as a multiple of standard deviation or IQR such that the number of hot moments is consistent among spatial replicates or among different years and that hot moments constitute only a small fraction of the observations (Stuchiner et al., 2025; Molodovskaya et al., 2012; Anthony and Silver, 2021, 2024; Li et al., 2015). The first method is preferred if the flux data follows a Gaussian-like distribution and the second method is more appropriate if the data is positively skewed due to spike-like events. In this study, the first method was used because the flux data appeared to show a normal distribution. The detection threshold was one standard deviation of daily flux in a given year. The number of hot moments detected with this threshold during the fertilization period was relatively stable, ranging from 9 in 2019 to 14 in 2022 (2020: 11; 2021: 13; 2023: 11; 2024: 10). A higher threshold of 1.5 times the standard deviation would result in a much larger interannual variation in the number hot moments during the fertilization period (from 5 in 2019 to 11 in 2022).

3. Results

3.1. Daily variations of N_2O fluxes and environmental factors

Fig. 1 shows the time series of daily N_2O and CO_2 fluxes, T_{soil}, and daily precipitation. The paddy growing season (May to October) experienced favorable hydrothermal conditions. Averaged over the period from 2019 to 2024, 57.5% of the annual precipitation occurred in the growing season, with a range of 48.1% (2022) to 80.1% (2021). Annual precipitation varied from 564.1 mm (2019) to 1321.6 mm (2020). The maximum daily precipitation (119.6 mm) occurred on July 19, 2023. The growing-season mean T_{soil} varied from 21.4 °C (2019) to 24.1 °C (2024) and the annual mean varied from 17.8 °C (2023) to 19.7 °C (2022).

The daily N_2O flux varied from −1.02 nmol m^{-2} s^{-1} (8 February 2021) to 6.83 nmol m^{-2} s^{-1} (4 September 2024). The N_2O flux was higher during the growing season under more favorable hydrothermal conditions, with an average daily value of 1.21 ± 0.94 nmol m^{-2} s^{-1}. In the non- growing season, the average daily N_2O flux was 0.94 ± 0.72 nmol m^{-2} s^{-1}. High daily N_2O emission fluxes tended to be accompanied by strong CO_2 absorption fluxes during the peak growing season (June to August; Fig. 1a and 1c).

3.2. Hot moments and controlling factors

Hot moments are shown in Fig.1a as red circles. These hot moments are days with the daily N_2O flux exceeding one standard deviation of all valid daily observations in the same year. On average, hot moments occurred in 14% of the observations and contributed 24% of the total N_2O emission. About 79% of the hot moments were observed in the growing season, and the rest in the non-growing season. Notably, 25% or 50 out of a total of 197 hot moments were observed during the paddy fertilization period (June to first half of July).

The N_2O flux increased with increasing T_{soil} during hot moments and non-hot moments (Fig. 2). The positive relationship between the N_2O flux and T_{soil} was stronger during non-hot moments (Fig. 2b, $R^2 = 0.75$) than hot moments (Fig. 2a, $R^2 = 0.34$). Some hot moments occurred in rainy conditions. To evaluate the impact of precipitation on N_2O emission, a flux difference (ΔN_2O) was calculated as the N_2O flux on the day of precipitation during a hot moment minus the mean daily N_2O flux from the previous three days. ΔN_2O was generally positive (Fig. 3); this is expected as the previous three days may or may not experience hot moments. The slight decreasing trend of ΔN_2O with increasing precipitation was not statistically significant ($p = 0.18$). This analysis was built on the approach of Miller et al. (2022), who calculated the difference in the N_2O flux between the rainfall day and the preceding day as a measure of precipitation impact on the flux. We also used the mean flux of one day and five days before a hot moment with rainfall as the reference to compute ΔN_2O. The relationship was not significant for either time windows ($R = 0.023$, $p = 0.91$ for one day; $R = -0.12$, $p = 0.50$ for five days).

There were 35 hot moments in rainy conditions and 162 in dry weather conditions. The mean hot-moment flux (2.53 ± 0.76 nmol m^{-2} s^{-1}) in rainy weather was not significantly different from the mean (2.55 ± 0.85 nmol m^{-2} s^{-1}) in dry weather ($p = 0.93$). In other words, precipitation was not the main trigger of hot moments in this paddy landscape.

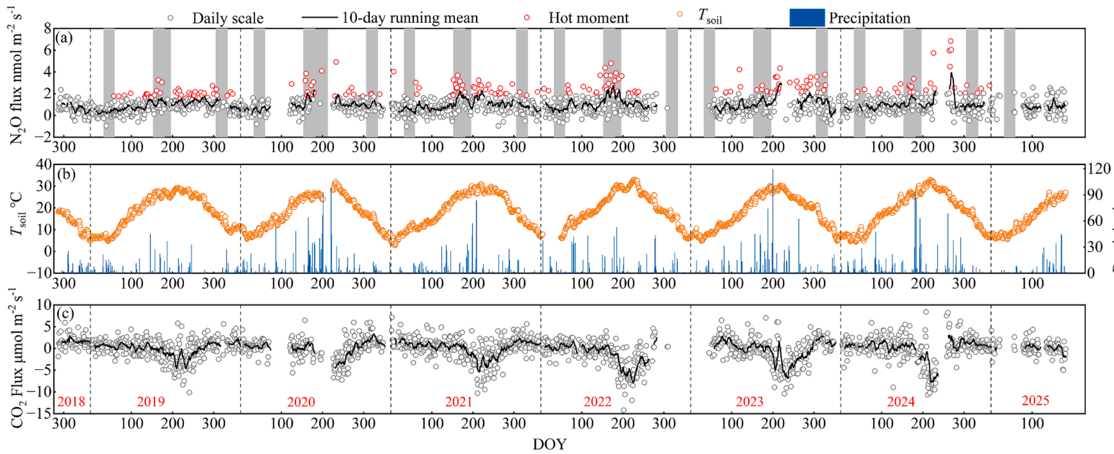

Fig. 1. Time series of (a) daily mean N_2O flux, 10-day running N_2O flux mean, and N_2O hot moments, (b) daily mean 10-cm soil temperature and daily precipitation, and (c) daily mean CO_2 flux. The gray shaded areas represent the fertilizer application periods.

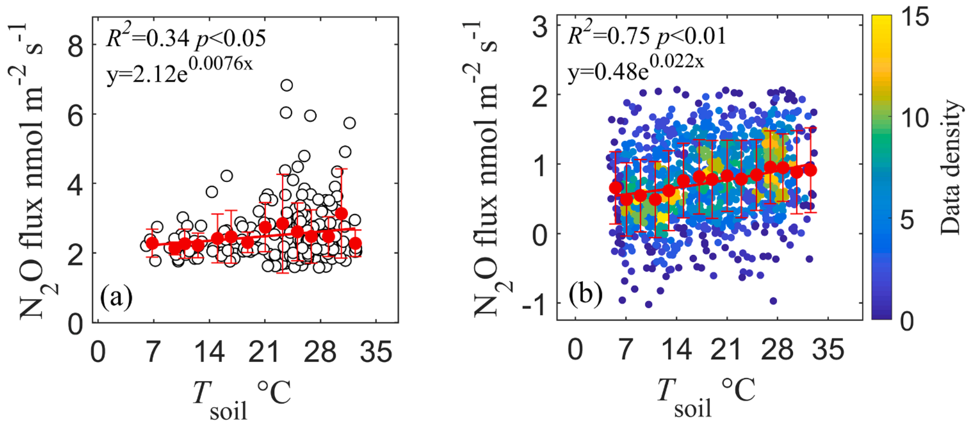

Fig. 2. Relationships between N_2O flux and T_{soil} during (a) hot moments and (b) non-hot moments of N_2O emission. Red curves represent exponential fits to 2 °C bin-averaged data (R^2 and p-values shown).

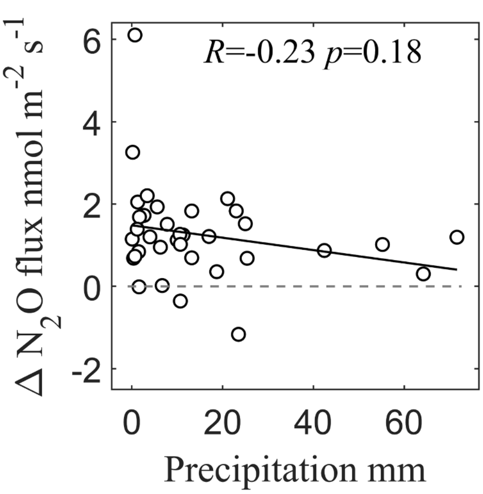

Fig. 3. Relationship between the N_2O flux enhancement during hot moments and cumulative precipitation during the three days leading to the hot moment.

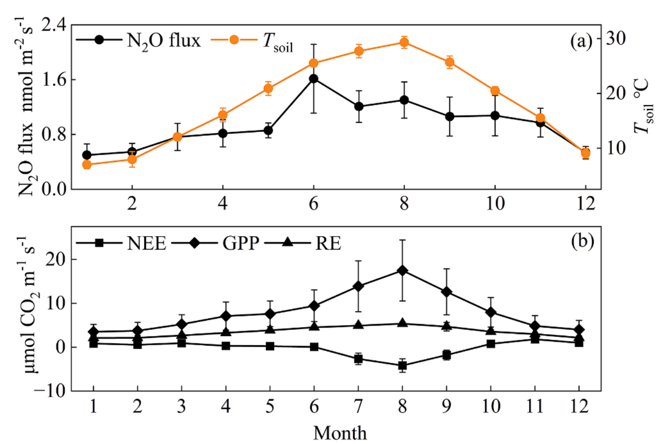

Fig. 4. (a) Monthly composite N_2O flux and soil temperature (T_{soil}), and (b) net ecosystem exchange (NEE), gross primary production (GPP), and ecosystem respiration (RE) from 2019 to 2024. The black line represents ± 1 standard deviation of multi-year observations.

3.3. Seasonal variations in N_2O and CO_2 fluxes

Fig. 4a shows the average monthly N_2O flux over the course of the year. The lowest monthly N_2O flux was 0.50 nmol m^{-2} s^{-1} (January) and the highest was 1.61 nmol m^{-2} s^{-1} (June) coinciding with paddy fertilization. A secondary peak occurred in August (1.30 nmol m^{-2} s^{-1}). The seasonal mean flux was highest in the summer (June, July, and August; 1.40 ± 0.41 nmol m^{-2} s^{-1}) and lowest in the winter (December, January, and February; 0.53 ± 0.12 nmol m^{-2} s^{-1}). The seasonal mean was 0.82 ± 0.16 in the spring (March, April, May) and 1.04 ± 0.26 nmol

m^{-2} s^{-1} in autumn (September, October., November).

The N_2O flux seasonality was not in sync with plant growth. The GPP peak occurred in August, two months later than the N_2O flux peak (Fig. 4b). On the monthly scale, the N_2O flux significantly increased with increasing GPP and decreased as NEE became less negative (Fig. S2), and the correlation with GPP was stronger than with NEE. Nitrogen fertilization resulted in N_2O flux peak in June. In August, paddy entered mid-growing season. GPP and RE reached their peaks at the time of highest T_{soil}.

3.4. Interannual variation in N_2O emission

The agricultural landscape acted as a CO_2 sink only in 2019, 2022 and 2023, whereas it was a CO_2 source in all other years (Table 1).

Table 1 lists the annual N_2O emission from 2019 to 2024, along with the annual footprint- weighted N input. The mean annual N_2O emission was 8.5 ± 0.5 kg N_2O—N ha^{-1} over the six years. The highest emission occurred in 2020, reaching 9.1 kg N_2O—N ha^{-1}, which accounted for 4.2% of the nitrogen input. The lowest emission occurred in 2019, with 7.6 kg N_2O—N ha^{-1}, representing 3.9% of the nitrogen input. For all years except 2019, the slope of the cumulative N_2O emission shows a sudden rise after May when the paddy transplant began (Fig. 5).

The interannual variability in the N_2O emission was weak, with a low CV of 5.9%. The annual precipitation was much more variable, with a CV of 25.1%, about four times that of the N_2O emission. The CV of N input was 6.6%, similar to the CV of annual N_2O emission. The multi-year mean emission factor was 4.3% ± 0.2%, with a low CV of 4.7%. Both the annual N_2O emission and the emission factor increased with increasing annual precipitation, but the relationships were not statistically significant (Fig. 6).

4. Discussion

4.1. Comparison of annual N_2O emission

Fig. 7 compares the annual N_2O emission observed in this study with those found in the literature. The literature results are grouped by spatial scale into three categories: landscape scale (~10 km) consisting of multiple dryland crop types, plot scale (~ 10 m) representing a fishpond, and field scale (~100 m) representing one site with a single crop (paddy) or rice-dry crop rotation. The mean annual N_2O emission of this study (8.5 ± 0.5 kg N_2O—N ha^{-1}) was 2.2 times higher than the mean value reported for dryland agricultural landscapes and fishponds and about twice that reported for paddy fields. Static chambers were used in the fishpond and paddy studies to measure the N_2O flux. Except for Hu et al. (2022), Zhou et al. (2018) and Yao et al. (2013), the observation frequency in these studies typically varied from twice a week to about once a week. It is likely that some hot moments were missed due to the low observational frequency. Hu et al. (2022) reported a high annual emission flux (7.8 kg N_2O—N ha^{-1}) for their field which was managed as a winter wheat-rice rotation system. Their system received high N input (200 kg N ha^{-1} for wheat and 250 kg N ha^{-1} for paddy). Moreover, they sampled more frequently (once per day) during fertilization, drainage, and post-precipitation periods, capturing short-term N_2O flux peaks.

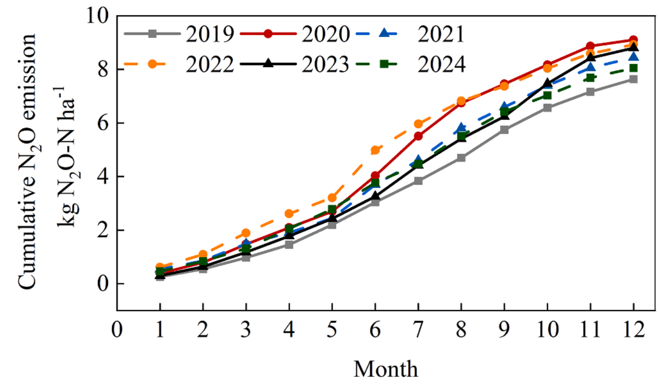

Fig. 5. The monthly cumulative N_2O emissions in the region.

For observational studies that covered three or more years, the CV is in the range of 19.4% - 106% for the annual N_2O emission, and 5.9% - 26.3% for annual precipitation (Table S1). In this study, the CV for annual precipitation was 25.1%, higher than in most other studies, yet the CV for annual N_2O emission was only 5.9%. The majority of the multi-year studies listed in Table S1 were conducted in fields and landscapes dominated by dryland crops, and precipitation is an important driver of interannual emission variability (Griffis et al., 2017). In comparison, precipitation is expected to play a weaker role in interannual emission variability in paddy fields, where intensive irrigation and prolonged flooding provide stable water input and maintain saturated soil moisture, thus buffering the effect of precipitation change (Zheng et al., 2000). The low emission CV in this study is consistent with this expectation.

However, the multi-year observations made by Zhou et al. (2018) in a paddy field and by Yao et al. (2013) in a field of rice-wheat rotation showed high interannual variability the in annual emission, with CV of 73.3% and 27.7%, respectively. To capture hot moments during high emission periods (e. g., the week after fertilizer application), the researchers measured the flux once a day using a flux chamber. At other times, measurements were made at a lower sampling frequency of 2–3 times per week. But hot moments can also occur in low emission periods (Tallec et al., 2022). For example, during the fallow season, Zhou et al. (2018) observed several hot moments when the flux was one order of magnitude greater than the baseline value. Given the low sampling frequency and the small area sampled by the chamber, some hot moments may have been missed, contributing to the interannual variability in these studies. We postulate that the EC observation in this study yielded a more robust estimate of the interannual variability because of its large measurement footprint and its continuous nature.

4.2. Comparison of patterns of hot moment

In dryland systems, hot moments can be triggered by fertilization

Table 1
Annual mean daily N_2O flux, annual mean daily CO_2 flux, annual T_{soil}, annual precipitation, annual N_2O emission, footprint-weighted N input, and emission factor from 2019 to 2024.

Time	Annual mean daily N_2O flux nmol m^{-2} s^{-1}	Annual mean daily CO_2 flux μmol m^{-2} s^{-1}	Annual T_{soil} °C	Annual precipitation mm	Annual N_2O emission kg N_2O—N ha^{-1}	N input kg N ha^{-1}	Emission Factor %
2019	0.90 ± 0.66	-0.050 ± 2.0	18.1	564.1	7.6	193	3.9
2020	0.95 ± 0.78	0.056 ± 2.40	18.2	1321.6	9.1	217	4.2
2021	0.95±0.85	0.11 ± 2.60	18.3	884.1	8.4	185	4.5
2022	1.06 ± 0.93	−1.32 ± 3.09	19.7	820.3	8.9	206	4.3
2023	1.11 ± 0.98	−0.36 ± 2.98	17.8	1073.1	8.8	203	4.3
2024	1.04 ± 1.00	0.043 ± 2.98	18.3	1114.6	8.0	179	4.4
Mean	0.99 ± 0.87	−0.25 ± 0.55	18.4		8.5 ± 0.5	197 ± 13	4.3 ± 0.2

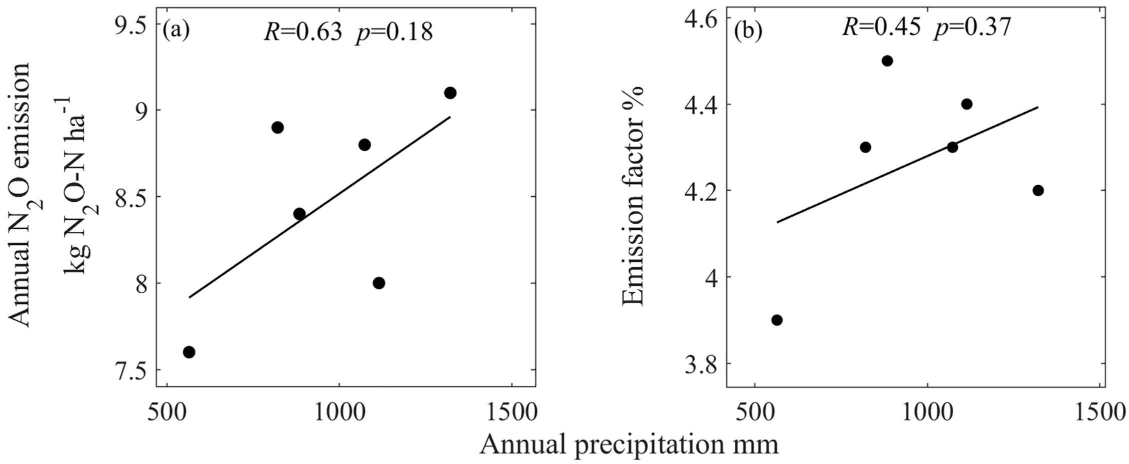

Fig. 6. Relationship of (a) annual N_2O emission and (b) emission factor with annual precipitation.

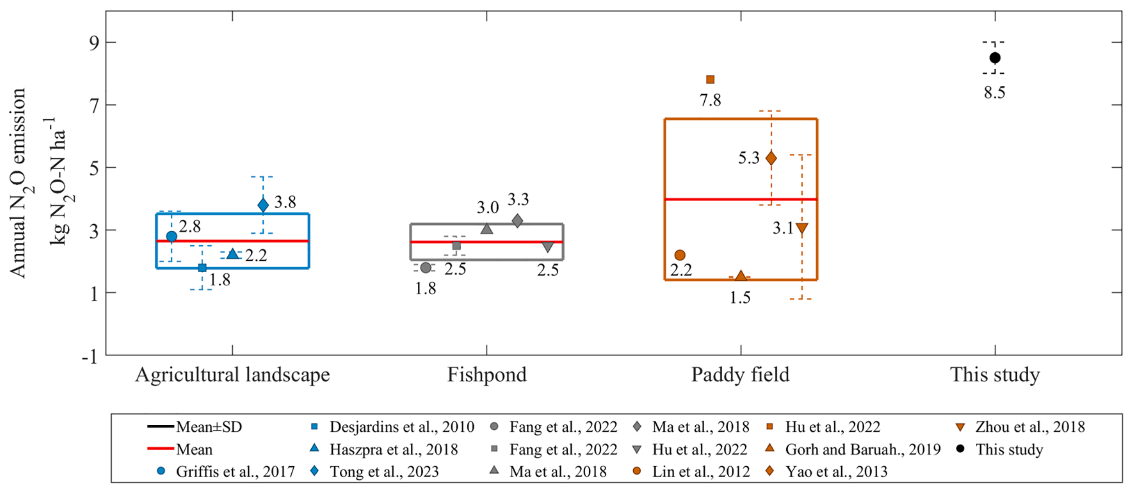

Fig. 7. Comparison of annual N_2O emission. Each datapoint represents the mean annual emission of one study, and error bars represents ± 1 standard deviation of interannual variation if multi-year data are available. Group means and standard deviations are given as horizontal lines and boxes (Desjardins et al., 2010; Haszpra et al., 2018; Tong et al., 2023; Fang et al., 2022; Ma et al., 2018; Lin et al., 2012; Hu et al., 2022; Gorh and Baruah, 2019; Yao et al., 2013; Zhou et al., 2018).

application (Stuchiner et al., 2025; Merbold et al., 2021; Li et al., 2015; Lognoul et al., 2019), precipitation events (Stuchiner et al., 2025; Anthony and Silver, 2021, 2024; Merbold et al., 2021; Li et al., 2015; Molodovskaya et al., 2012; Lognoul et al., 2019), soil temperature fluctuations (Stuchiner et al., 2025; Anthony and Silver, 2021, 2024; Merbold et al., 2021; Lognoul et al., 2019), and freeze/thaw cycles (Wagner-Riddle et al., 2007; Molodovskaya et al., 2012; Stuchiner et al., 2025). They occur in 1–20% of the time, but their contribution to the annual N_2O emission often exceeds 40%. In this study, hot moments occurred in 14% of the time, and their contribution to the annual N_2O emission was 24%, which was lower than that reported for most dryland ecosystems. Here, triggers of hot moment were not well-defined. Freeze/thaw was not a factor as the soil did not freeze during the experiment (Fig. 1b). That the flux during hot moments had a weaker correlation with temperature than that in other times (Fig. 2) suggests that temperature fluctuations did not play a major role. We pointed out earlier (Section 3.2) that hot moments in rainy and fair weather were about equal in strength. It is possible that precipitation was a hot moment trigger, but its effect may have been concealed or diluted by the irrigation water standing in the paddy fields.

In the month of fertilizer application (June), hot moment occurrence time fraction was 33%, which is more than twice the mean occurrence fraction of 14%. The mean hot moment flux in June was 2.67 nmol m^{-2} s^{-1}, which was 187% higher than the mean flux of non-hot moments (0.93 nmol m^{-2} s^{-1}) in June. The mean flux in June (1.61 nmol m^{-2} s^{-1}) was greater than that in the month before (May; 0.86 nmol m^{-2} s^{-1}) and after (July; 1.21 nmol m^{-2} s^{-1}). So, fertilizer application clearly enhanced the emission. But fertilizer application as a trigger of hot moment was somewhat muted. The flux footprint encompassed a larger number of fields where fertilization was not synchronized, with time differences of several weeks. Varied fertilization timing and management practice prevented hot moments from concentrating in time and reaching a spike-like high flux intensity.

4.3. Emission factor

The N_2O emission factor remained stable (mean 4.3%; CV = 4.7%) despite significant interannual fluctuations in precipitation (CV = 25.1%). This value is much higher than the IPCC direct emission factor for dryland crops (1%) and paddy fields (0.4%) (IPCC, 2019). In a meta analysis of 67 paddy field observations in China, Aliyu et al. (2019) obtained a mean emission factor of 0.48 ± 0.05%, which is much lower than the emission factor in this study. Five factors may have contributed to the difference. First, Aliyu et al. (2019) used the difference in the annual N_2O flux between fertilized plots and a background flux in control plots without fertilizer application to compute the emission factor, while in this study, the flux included the background component. According to Aliyu et al. (2019), the mean background flux is 0.43 kg

N_2O—N ha^{-1} for rice paddies. Removing this background from the overall annual emission would reduce our emission factor slightly to 4.1 ± 0.2%. Second, some of the flux data analyzed by Aliyu et al. (2019) were derived from soil chambers, which can only measure soil emission. There is evidence that crop plants can emit N_2O by serving as passive conduits of N_2O from the soil to the atmosphere (Zhang et al., 2015; Chang et al., 1998; Chen et al., 1997; Yu et al., 1997). Zhang et al. (2015) observed that the plant flux accounts for 12% of the ecosystem N_2O flux in a soybean field. The role of rice plant transport of CH_4 to the atmosphere has been widely recognized (e.g., Wassmann and Aulakh, 2000). Yu et al. (1997) showed that rice plants account for 85.7% of total N_2O emission to the atmosphere through the plant aerenchyma while the flux across the soil-water interface plays a minor role. Third, having small basal areas and being operated infrequently, the flux chambers in those studies may have missed some emission hotspots and hot moments (e.g., Audet et al., 2014), causing low biases in the emission factor estimates. The rates of emission from hotspots are 2-fold greater than non-hotspot locations in a corn field (Turner et al., 2016). Fourth, the N input used for our emission calculation did not include the contribution of atmospheric N deposition. The total N deposition (wet plus dry) is about 40 kg N ha^{-1} yr^{-1} in Eastern China (Yu et al., 2019). Addition of this to the N input would reduce our multi-year mean emission factor to 3.6 ± 0.1%. Finally, flux chambers can only detect direct emission, whereas the EC flux measured on the 70-m tower consisted of both direct emission from paddy fields and indirect emissions from drainage networks. According to IPCC, the indirect emission factor for cropland is 1.1% (IPCC, 2019).

One source of uncertainty is N input. The N input data for 2019 came from a survey of local farmers and was more accurate than the N input data for the subsequent years which were scaled by county-level data (Section 2.1). This uncertainty may have influenced the interannual variability of the emission factor, but the general conclusion should be robust because the emission factor for 2019 is much higher than the IPCC default value.

Our emission factor is in better agreement with other “top-down” estimates. Crutzen et al. (2008) estimated that the global N_2O emission factor, including both direct and indirect emissions related to anthropogenic N inputs, is 4% ± 1%. Using boundary-layer methods and N_2O concentration measured on a tall tower, Griffis et al. (2017) obtained an emission factor of 5.3% ± 1.2% for the U.S. Corn Belt. Wagner-Riddle et al. (2007) used the flux-gradient method to make observation of the annual N_2O flux of wheat and corn crops under conventional management in southern Ontario, Canada. Dividing their annual flux values by the corresponding N inputs yields an emission factor of about 3%.

5. Conclusions

This study presents six years (2019–2024) of near-continuous and high-frequency N_2O observation in a paddy-dominated agricultural landscape using a tall-tower eddy covariance system. N_2O emission hot moments mostly occurred during the paddy growing season (May to October). The application of fertilizer in June stimulated N_2O emission, resulting in a marked emission peak. The mean annual N_2O emission was 8.5 ± 0.5 kg N_2O—N $ha^{-1}yr^{-1}$. Despite high variability in annual precipitation (CV = 25.1%), the annual N_2O emission showed minimal interannual variation (CV = 5.9%), indicating weak role of precipitation in influencing N_2O emission. The overall emission factor was 4.3% ± 0.2%, which was much higher than most published studies for paddy rice and the IPCC-recommended values for direct and indirect emission. Possible reasons for this difference included N deposition, emission by rice plants and indirect emission from drainage networks in the tower flux footprint.

This study was conducted in a landscape managed as a single-cropping paddy cultivation with a specific irrigation regime (flooding–drainage–reflooding–moderate irrigation without waterlogging) and in a specific climate (subtropical monsoon climate). Caution is warranted when extrapolating the findings to other paddy systems or climatic regions. Long-term EC observations of N_2O flux remain limited for paddy rice. Future research should integrate EC measurements with chamber sampling to better capture N_2O hot moments (e.g., during fertilization and drainage), to clarify the role of plant transport of N_2O to the atmosphere, and to quantify indirect N_2O emission associated with irrigation and drainage networks, and should investigate methodological discrepancies between chamber-based and EC-based estimates to improve flux upscaling.

CRediT authorship contribution statement

Jie Shi: Writing – original draft, Software, Methodology, Investigation, Formal analysis, Data curation, Conceptualization. **Mi Zhang:** Writing – review & editing, Supervision, Project administration, Methodology, Funding acquisition, Conceptualization. **Wei Xiao:** Supervision, Project administration, Funding acquisition, Conceptualization. **Yanhong Xie:** Software, Methodology, Investigation, Data curation. **Yang He:** Investigation, Formal analysis. **Hengxin Bao:** Investigation, Formal analysis, Data curation. **Fuyu Yang:** Investigation, Formal analysis. **Shenbao Zhang:** Investigation. **Xuhui Lee:** Writing – review & editing, Methodology, Conceptualization.

Declaration of competing interest

The authors declare that they have no known competing financial interests or personal relationships that could have appeared to influence the work reported in this paper.

Acknowledgements

This work was supported by the 333 Project of Jiangsu Province [grant number BRA2022023], the National Natural Science Foundation of China [grant number U24A20590, 42021004], the Joint funds of the Zhejiang Provincial Natural Science Foundation of China (grant number LZJMZ23D050002), and the Postgraduate Research & Practice Innovation Program of Jiangsu Province (grant number KYCX24_1450).

Supplementary materials

Supplementary material associated with this article can be found, in the online version, at doi:10.1016/j.agrformet.2026.111451.

Data availability

Data will be made available on request.

References

Aliyu, G., Luo, J., Di, H., Lindsey, S., Liu, D., Yuan, J., Chen, Z., Lin, Y., He, Y., Zaman, M., Ding, W., 2019. Nitrous oxide emissions from China's croplands based on regional and crop-specific emission factors deviate from IPCC 2006 estimates. Sci. Total Environ. 669, 547–558. https://doi.org/10.1016/j.scitotenv.2019.03.142.

Anthony, T.L., Silver, W.L., 2021. Hot moments drive extreme nitrous oxide and methane emissions from agricultural peatlands. Glob. Change Biol. 27, 5141–5153. https://doi.org/10.1111/gcb.15802.

Anthony, T.L., Silver, W.L., 2024. Hot spots and hot moments of greenhouse gas emissions in agricultural peatlands. Biogeochemistry 167, 461–477. https://doi.org/10.1007/s10533-023-01095-y.

Aubinet, M., Vesala, T., Papale, D., 2012. Eddy Covariance: a Practical Guide to Measurement and Data Analysis. Springer.

Audet, J., Hoffmann, C.C., Andersen, P.M., Baattrup-Pedersen, A., Johansen, J.R., Larsen, S.E., Kjaergaard, C., Elsgaard, L., 2014. Nitrous oxide fluxes in undisturbed riparian wetlands located in agricultural catchments: emission, uptake and controlling factors. Soil Biol. Biochem. 68, 291–299. https://doi.org/10.1016/j.soilbio.2013.10.011.

Barczyk, L., Six, J., Ammann, C., 2024. Partitioning and driver analysis of eddy covariance derived N_2O emissions from a grazed and fertilized pasture. Agric. For. Meteorol. 359, 110278. https://doi.org/10.1016/j.agrformet.2024.110278.

Bernhardt, E.S., Blaszczak, J.R., Ficken, C.D., Fork, M.L., Kaiser, K.E., Seybold, E.C., 2017. Control points in ecosystems: moving beyond the hot spot hot moment concept. Ecosystems 20, 665–682. https://doi.org/10.1007/s10021-016-0103-y.

Cai, Z., Xing, G., Yan, X., Xu, H., Tsuruta, H., Yagi, K., Minami, K., 1997. Methane and nitrous oxide emissions from rice paddy fields as affected by nitrogen fertilisers and water management. Plant Soil 196, 7–14. https://doi.org/10.1023/A:1004263405020.

Chang, C., Janzen, H.H., Cho, C.M., Nakonechny, E.M., 1998. Nitrous oxide emission through plants. Soil Sci. Soc. Am. J. 62, 35–38. https://doi.org/10.2136/sssaj1998.03615995006200010005x.

Chen, G.X., Huang, G.H., Huang, B., Yu, K.W., Wu, J., Xu, H., 1997. Nitrous oxide and methane emissions from soil–plant systems. Nutr. Cycl. Agroecosyst. 49, 41–45. https://doi.org/10.1023/a:1009758900629.

Chen, Z., Xu, Y., Zhou, X., Tang, J., Kuzyakov, Y., Yu, H., Fan, J., Ding, W., 2017. Extreme rainfall and snowfall alter responses of soil respiration to nitrogen fertilization: a 3-year field experiment. Glob. Change Biol. 23, 3403–3417. https://doi.org/10.1111/gcb.13620.

Crutzen, P.J., Mosier, A.R., Smith, K.A., Winiwarter, W., 2008. N2O release from agro-biofuel production negates global warming reduction by replacing fossil fuel. Atmos. Chem. Phys. 8, 389–395. https://doi.org/10.5194/acp-8-389-2008.

Desjardins, R.L., Pattey, E., Smith, W.N., Worth, D., Grant, B., Srinivasan, R., MacPherson, J.I., Mauder, M., 2010. Multiscale estimates of N_2O emissions from agricultural lands. Agric. For. Meteorol. 150, 817–824. https://doi.org/10.1016/j.agrformet.2009.09.001.

Fang, X., Zhao, J., Wu, S., Yu, K., Huang, J., Ding, Y., Hu, T., Xiao, S., Liu, S., Zou, J., 2022. A two-year measurement of methane and nitrous oxide emissions from freshwater aquaculture ponds: affected by aquaculture species, stocking and water management. Sci. Total Environ. 813, 151863. https://doi.org/10.1016/j.scitotenv.2021.151863.

Gong, P., Liu, H., Zhang, M., Li, C., Wang, J., Huang, H., Clinton, N., Ji, L., Li, W., Bai, Y., Chen, B., Xu, B., Zhu, Z., Yuan, C., Suen, H., Guo, J., Nan, X., Li, W., Zhao, Y., Yang, J., Yu, C., Wang, X., Fu, H., Yu, L., Dronova, I., Hui, F., Cheng, X., Shi, X., Xiao, F., Liu, Q., Song, L., 2019. Stable classification with limited sample: transferring a 30-m resolution sample set collected in 2015 to mapping 10-m resolution global land cover in 2017. Sci. Bull. 64, 370–373. https://doi.org/10.1016/j.scib.2019.03.002.

Gorh, D., Baruah, K.K., 2019. Estimation of methane and nitrous oxide emission from wetland rice paddies with reference to global warming potential. Environ. Sci. Pollut. Res. 26, 16331–16344. https://doi.org/10.1007/s11356-019-05026-z.

Griffis, T.J., Chen, Z., Baker, J.M., Wood, J.D., Millet, D.B., Lee, X., Venterea, R.T., Turner, P.A., 2017. Nitrous oxide emissions are enhanced in a warmer and wetter world. Proc. Natl. Acad. Sci. 114, 12081–12085. https://doi.org/10.1073/pnas.1704552114.

Griffis, T.J., Lee, X., Baker, J.M., Russelle, M.P., Zhang, X., Venterea, R., Millet, D.B., 2013. Reconciling the differences between top-down and bottom-up estimates of nitrous oxide emissions for the U.S. Corn Belt. Glob. Biogeochem. Cycles. 27, 746–754. https://doi.org/10.1002/gbc.20066.

Haszpra, L., Hidy, D., Taligás, T., Barcza, Z., 2018. First results of tall tower based nitrous oxide flux monitoring over an agricultural region in Central Europe. Atmos. Environ. 176, 240–251. https://doi.org/10.1016/j.atmosenv.2017.12.035.

Hu, Z., Gu, C., Maucieri, C., Shi, F., Zhao, Y., Feng, C., Cao, Y., Zhang, Y., 2022. Crayfish–fish aquaculture ponds exert reduced climatic impacts and higher economic benefits than traditional wheat–rice paddy cultivation. Agriculture 12, 515. https://doi.org/10.3390/agriculture12040515.

IPCC, 2006. IPCC guidelines for national greenhouse gas inventories, prepared by the national greenhouse gas inventories programme, Eggleston H.S., Buendia L., Miwa K., Ngara T. and Tanabe K. (eds). IGES, Japan. https://www.ipccnggip.iges.or.jp/public/2006gl/vol4.html.

IPCC, 2019. 2019 Refinement to the 2006 IPCC Guidelines for National Greenhouse Gas Inventories, Calvo Buendia, E., Tanabe, K., Kranjc, A., Baasansuren, J., Fukuda, M., Ngarize S., Osako, A., Pyrozhenko, Y., Shermanau, P. and Federici, S. (eds). IPCC, Switzerland. https://www.ipcc-nggip.iges.or.jp/public/2019rf/vol4.html.

Kljun, N., Calanca, P., Rotach, M.W., Schmid, H.P., 2015. A simple two-dimensional parameterisation for flux footprint prediction (FFP). Geosci. Model Dev. 8, 3695–3713. https://doi.org/10.5194/gmd-8-3695-2015.

Kroon, P.S., Schrier-Uijl, A.P., Hensen, A., Veenendaal, E.M., Jonker, H.J.J., 2010. Annual balances of CH_4 and N_2O from a managed fen meadow using eddy covariance flux measurements. Eur. J. Soil Sci. 61, 773–784. https://doi.org/10.1111/j.1365-2389.2010.01273.x.

Li, M., Shimizu, M., Hatano, R., 2015. Evaluation of N2O and CO2 hot moments in managed grassland and cornfield, southern Hokkaido, Japan. CATENA. 133, 1–13. https://doi.org/10.1016/j.catena.2015.04.014.

Lin, S., Iqbal, J., Hu, R., Ruan, L., Wu, J., Zhao, J., Wang, P., 2012. Differences in nitrous oxide fluxes from red soil under different land uses in mid-subtropical China. Agric. Ecosyst. Environ. 146, 168–178. https://doi.org/10.1016/j.agee.2011.10.024.

Lognoul, M., Debacq, A., De Ligne, A., Dumont, B., Manise, T., Bodson, B., Heinesch, B., Aubinet, M., 2019. N_2O flux short-term response to temperature and topsoil disturbance in a fertilized crop: An eddy covariance campaign. Agric. For. Meteorol. 271, 193–206. https://doi.org/10.1016/j.agrformet.2019.02.033.

Ma, Y., Sun, L., Liu, C., Yang, X., Zhou, W., Yang, B., Schwenke, G., Liu, D., 2018. A comparison of methane and nitrous oxide emissions from inland mixed-fish and crab aquaculture ponds. Sci. Total Environ. 637-638, 517–523. https://doi.org/10.1016/j.scitotenv.2018.05.040.

Mauder, M., Foken, T., 2004. Documentation and instruction manual of the Eddy Covariance software Package TK2. University of Bayreuth, Department of Micrometeorology Arbeitsergebnisse Nr. 6, 42.

McClain, M.E., Boyer, E.W., Dent, C.L., Gergel, S.E., Grimm, N.B., Groffman, P.M., Hart, S.C., Harvey, J.W., Johnston, C.A., Mayorga, E., McDowell, W.H., Pinay, G., 2003. Biogeochemical hot spots and hot moments at the interface of terrestrial and aquatic ecosystems. Ecosystems 6, 301–312. https://doi.org/10.1007/s10021-003-0161-9.

Merbold, L., Decock, C., Eugster, W., Fuchs, K., Wolf, B., Buchmann, N., Hörtnagl, L., 2021. Are there memory effects on greenhouse gas emissions (CO_2, N_2O and CH_4) following grassland restoration? Biogeosciences 18, 1481–1498. https://doi.org/10.5194/bg-18-1481-2021.

Miller, L.T., Griffis, T.J., Erickson, M.D., Turner, P.A., Deventer, M.J., Chen, Z., Yu, Z., Venterea, R.T., Baker, J.M., Frie, A.L., 2022. Response of nitrous oxide emissions to individual rain events and future changes in precipitation. J. Environ. Qual. 51, 312–324. https://doi.org/10.1002/jeq2.20348.

Molodovskaya, M., Singurindy, O., Richards, B.K., Warland, J., Johnson, M.S., Steenhuis, T.S., 2012. Temporal variability of nitrous oxide from fertilized croplands: hot moment analysis. Soil Sci. Soc. Am. J. 76, 1728–1740. https://doi.org/10.2136/sssaj2012.0039.

Moncrieff, J.B., Massheder, J.M., de Bruin, H., Elbers, J., Friborg, T., Heusinkveld, B., Kabat, P., Scott, S., Soegaaed, H., Verhoef, A., 1997. A system to measure surface fluxes of momentum, sensible heat, water vapor and carbon dioxide. J. Hydrol. 188-189, 589–611. https://doi.org/10.1016/S0022-1694(96)03194-0.

Scanlon, T., Kiely, G., 2003. Ecosystem-scale measurements of nitrous oxide fluxes for an intensely grazed, fertilized grassland. Geophys. Res. Lett. 30. https://doi.org/10.1029/2003GL017454.

Stuchiner, E.R., Xu, J., Eddy, W.C., DeLucia, E.H., Yang, W.H., 2025. Hot or not? An evaluation of methods for identifying hot moments of nitrous oxide emissions from soils. J. Geophys. Res. Biogeosci. 130. https://doi.org/10.1029/2024JG008138.

Tallec, T., Bigaignon, L., Delon, C., Brut, A., Ceschia, E., Mordelet, P., Zawilski, B., Granouillac, F., Claverie, N., Fieuzal, R., Lemaire, B., Le Dantec, V., 2022. Dynamics of nitrous oxide emissions from two cropping systems in southwestern France over 5 years: cross impact analysis of heterogeneous agricultural practices and local climate variability. Agric. For. Meteorol. 323, 109093. https://doi.org/10.1016/j.agrformet.2022.109093.

Tian, H., Pan, N., Thompson, R.L., Canadell, J.G., Suntharalingam, P., Regnier, P., Davidson, E.A., Prather, M., Ciais, P., Muntean, M., Pan, S., Winiwarter, W., Zaehle, S., Zhou, F., Jackson, R.B., Bange, H.W., Berthet, S., Bian, Z., Bianchi, D., Bouwman, A.F., Buitenhuis, E.T., Dutton, G., Hu, M., Ito, A., Jain, A.K., Jeltsch-Thömmes, A., Joos, F., Kou-Giesbrecht, S., Krummel, P.B., Lan, X., Landolfi, A., Lauerwald, R., Li, Y., Lu, C., Maavara, T., Manizza, M., Millet, D.B., Mühle, J., Patra, P.K., Peters, G.P., Qin, X., Raymond, P., Resplandy, L., Rosentreter, J.A., Shi, H., Sun, Q., Tonina, D., Tubiello, F.N., van der Werf, G.R., Vuichard, N., Wang, J., Wells, K.C., Western, L.M., Wilson, C., Yang, J., Yao, Y., You, Y., Zhu, Q., 2024. Global nitrous oxide budget (1980–2020). Earth Syst. Sci. Data 16, 2543–2604. https://doi.org/10.5194/essd-16-2543-2024.

Tian, H., Xu, R., Canadell, J.G., Thompson, R.L., Winiwarter, W., Suntharalingam, P., Davidson, E.A., Ciais, P., Jackson, R.B., Janssens-Maenhout, G., Prather, M.J., Regnier, P., Pan, N., Pan, S., Peters, G.P., Shi, H., Tubiello, F.N., Zaehle, S., Zhou, F., Arneth, A., Battaglia, G., Berthet, S., Bopp, L., Bouwman, A.F., Buitenhuis, E.T., Chang, J., Chipperfield, M.P., Dangal, S.R.S., Dlugokencky, E., Elkins, J.W., Eyre, B. D., Fu, B., Hall, B., Ito, A., Joos, F., Krummel, P.B., Landolfi, A., Laruelle, G.G., Lauerwald, R., Li, W., Lienert, S., Maavara, T., MacLeod, M., Millet, D.B., Olin, S., Patra, P.K., Prim, R.G., Raymond, P.A., Ruiz, D.J., van der Werf, G.R., Vuichard, N., Wang, J., Weiss, R.F., Wells, K.C., Wilson, C., Yang, J., Yao, Y., 2020. A comprehensive quantification of global nitrous oxide sources and sinks. Nature 586, 248–256. https://doi.org/10.1038/s41586-020-2780-0.

Tong, X., Scheeren, B., Bosveld, F., Hensen, A., Frumau, A., Meijer, H.A.J., Chen, H., 2023. Magnitude and seasonal variation of N_2O and CH_4 emissions over a mixed agriculture-urban region. Agric. For. Meteorol. 334, 109433. https://doi.org/10.1016/j.agrformet.2023.109433.

Turner, P.A., Griffis, T.J., Mulla, D.J., Baker, J.M., Venterea, R.T., 2016. A geostatistical approach to identify and mitigate agricultural nitrous oxide emission hotspots. Sci. Total Environ. 572, 442–449. https://doi.org/10.1016/j.scitotenv.2016.08.094.

van Beek, C.L., Pleijter, M., Kuikman, P.J., 2011. Nitrous oxide emissions from fertilized and unfertilized grasslands on peat soil. Nutr. Cycl. Agroecosyst. 89, 453–461. https://doi.org/10.1007/s10705-010-9408-y.

Vickers, D., Mahrt, L., 1997. Quality control and flux sampling problems for tower and aircraft data. J. Atmos. Ocean. Technol. 14, 512–526. https://doi.org/10.1175/1520-0426(1997)014<0512:QCAFSP>2.0.CO;2.

Wagner-Riddle, C., Baggs, E.M., Clough, T.J., Fuchs, K., Petersen, S.O., 2020. Mitigation of nitrous oxide emissions in the context of nitrogen loss reduction from agroecosystems: managing hot spots and hot moments. Curr. Opin. Environ. Sustain. 47, 46–53. https://doi.org/10.1016/j.cosust.2020.08.002.

Wagner-Riddle, C., Furon, A., Mclaughlin, N.L., Lee, I., Barbeau, J., Jayasundara, S., Parkin, G., Von Bertoldi, P., Warland, J., 2007. Intensive measurement of nitrous oxide emissions from a corn–soybean–wheat rotation under two contrasting management systems over 5 years. Glob. Change Biol. 13, 1722–1736. https://doi.org/10.1111/j.1365-2486.2007.01388.x.

Wang, H., Zhang, Q., Li, X., Yi, Y., Wang, Q., Gao, L., Wang, J., He, D., Li, M., 2023. Surface microrelief induced by tillage management alters the pathway and composition of dissolved organic matter exports from soils to runoff during rainfall. Water Res. 245, 120554. https://doi.org/10.1016/j.watres.2023.120554.

Wang, J., Liu, Q., Zhao, S., He, S., Yang, B., Wang, N., Hou, P., Xue, L., Yang, L., 2024. Heavy rainfall stimulates more N_2O emissions from wheat fields during basal and overwintering fertilization phases. Agric. Ecosyst. Environ. 376, 109227. https://doi.org/10.1016/j.agee.2024.109227.

Wassmann, R., Aulakh, M.S., 2000. The role of rice plants in regulating mechanisms of methane emissions. Biol. Fertil. Soils 31, 20–29. https://doi.org/10.1007/s003740050619.

Xie, Y., Zhang, M., Xiao, W., Zhao, J., Huang, W., Zhang, Z., Hu, Y., Qin, Z., Jia, L., Pu, Y., Chu, H., Wang, J., Shi, J., Liu, S., Lee, X., 2022. Nitrous oxide flux observed with tall-tower eddy covariance over a heterogeneous rice cultivation landscape. Sci. Total Environ. 810. https://doi.org/10.1016/j.scitotenv.2021.152210.

Yao, Z., Zheng, X., Wang, R., Dong, H., Xie, B., Mei, B., Zhou, Z., Zhu, J., 2013. Greenhouse gas fluxes and NO release from a Chinese subtropical rice-winter wheat rotation system under nitrogen fertilizer management. J. Geophys. Res. Biogeosci. 118, 623–638. https://doi.org/10.1002/jgrg.20061.

Yu, G., Jia, Y., He, N., Zhu, J., Chen, Z., Wang, Q., Piao, S., Liu, X., He, H., Guo, X., Wen, Z., Li, P., Ding, G., Goulding, K., 2019. Stabilization of atmospheric nitrogen deposition in China over the past decade. Nat. Geosci. 12, 424–429. https://doi.org/10.1038/s41561-019-0352-4.

Yu, K., Wang, Z., Chen, G., 1997. Nitrous oxide and methane transport through rice plants. Biol. Fertil. Soils 24, 341–343. https://doi.org/10.1007/s003740050254.

Zhang, X., Lee, X., Griffis, T.J., Andrews, A.E., Baker, J.M., Erickson, M.D., Hu, N., Xiao, W., 2015. Quantifying nitrous oxide fluxes on multiple spatial scales in the Upper Midwest. USA. Int. J. Biometeorol. 59, 299–310. https://doi.org/10.1007/s00484-014-0842-4.

Zheng, X., Wang, M., Wang, Y., Shen, R., Gou, J., Ling, L., Jin, J., Li, L., 2000. Impacts of soil moisture on nitrous oxide emission from croplands: a case study on the rice-based agro-ecosystem in Southeast China. Chemosphere Glob. Change Sci. 2, 207–224. https://doi.org/10.1016/S1465-9972(99)00056-2.

Zhou, M., Wang, X., Wang, Y., Zhu, B., 2018. A three-year experiment of annual methane and nitrous oxide emissions from the subtropical permanently flooded rice paddy fields of China: emission factor, temperature sensitivity and fertilizer nitrogen effect. Agric. For. Meteorol. 250-251, 299–307. https://doi.org/10.1016/j.agrformet.2017.12.265.